INDONESIAN JOURNAL ON GEOSCIENCE
Geological Agency
Ministry of Energy and Mineral Resources

Journal homepage: http://ijog.geologi.esdm.go.id
ISSN 2355-9314, e-ISSN 2355-9306

Geothermal Surface Manifestation Identification Using Airborne Hyperspectral Imagery Case Study: Davis-Schrimpf Geothermal Field, Salton Sea, California

[1]Izzul Qudsi and [2]Muhammad Rifat Noor

[1]Geovartha, Indonesia
[2]Badan Pengkajian dan Penerapan Teknologi (BPPT), Indonesia

Corresponding author: izzul.qudsi@gmail.com
Manuscript received: December, 31, 2020; revised: March, 28, 2021;
approved: June, 11, 2021; available online: February, 18, 2022

Abstract - Research on surface geothermal evidence has been done extensively using remote sensing techniques. For detailed remote sensing exploration on geothermal areas, UAV and airborne based were preferred over the satellite-based sensor. In this research, anomalies in surface temperature, mineral occurrence, and ammonia emission were studied on a set of airborne hyperspectral imagery from NASA, the Hyperspectral Thermal Emission Spectrometer (HyTES). High-resolution surface temperature and mineral maps were able to identify and describe the mineralogy of the mud pots and gryphons at the Davis-Schrimpf Geothermal Field, Salton Sea, California. From the surface temperature map, the surface temperature of the geothermal features wa s measured at approximately 314°K (40°C) and higher. The purest pixels from MNF transformation of the first four cleanest bands of emissivity map produce endmembers that include the geothermal indicator minerals (barite, anhydrite, quartz, gypsum). Based on the mineralogy deposits, these manifestations are classified as potassic alteration types from a porphyry system that could be an indication of an active geothermal system. This also explains that the surface features are part of the upper reservoir of the Salton Sea Geothermal Field. On the other hand, ammonia detection that was performed in this research failed to get any clear recognition from the simple image processing. It is concluded that the airborne hyperspectral imagery could be a reliable option for remote sensing geothermal exploration, as it was able to characterize the surface geothermal manifestation with quite good detail using this imagery from a wide area of survey.

Keywords: geothermal, remote sensing, HyTES, mineral mapping, surface manifestation

How to cite this article:
Qudsi, I. and Noor, M.R., 2022. Geothermal Surface Manifestation Identification Using Airborne Hyperspectral Imagery Case Study: Davis-Schrimpf Geothermal Field, Salton Sea, California. *Indonesian Journal on Geoscience*, 9 (1), p.119-130. DOI: 10.17014/ijog.9.1.119-130

Introduction

Background

Remote sensing has been used in many geothermal exploration studies. Not only to identify several direct evidences such as the occurrence of the caldera, hot springs, or other surface geothermal manifestations, indirect proof such as surface temperature could also be mapped using the various wavelength ranges from camera sensors. Der Meer *et al*. (2014) published a comprehensive review of the usability of the application of geological remote sensing for geothermal exploration.

There are three types of remote sensing platforms, satellite, airborne, and Unmanned Aerial Vehicles (UAV), each type has its strength and limitation. Satellite-based imagery costs the lowest

compared to the other two platforms. However, the coarser image resolution is a major drawback to be used in a surface geothermal manifestation identification, because most of the manifestations are smaller than the size of a single-pixel from satellite imagery (30 m or higher). Several studies using UAV (Harvey and Luketina, 2014; Nishar *et al*., 2016) and airborne (Ramdhan, 2019) platforms were able to capture the surface features with the designated image resolution.

The UAV campaign surely costs much lower than the airborne flight, but this could only be applicable to a small and reachable area. In Indonesia, there are plenty of large and remote geothermal areas that need to be discovered. For this reason, this paper is focusing on airborne hyperspectral imagery to find the surface geothermal manifestation.

A set of open source datasets from NASA airborne hyperspectral campaigns on a geothermal field, the Hyperspectral Thermal Emission Spectrometer (HyTES) imagery of Salton Sea, was used as the case study material in this paper. From this image, the mineral deposit concept on identifying the active geothermal system by Bogie *et al.* (2000) was adapted to define the surface geothermal features. A previous remote sensing study by Reath (2011) combining the information from SEBASS and ASTER imageries with SEM and XRD was able to identify the geothermally related minerals at the Salton Sea.

This paper aims for a similar result using HyTES imagery, but more focusing on characterizing the features in a smaller area (Davis-Schrimpf Field). Another research objective is also added to identify the occurrence of ammonia using several simple image processing techniques. Field information from past studies were used to confirm the findings.

Geological/Stratigraphic Settings

The Salton Sea Geothermal Field is located at the Salton Sea in southern California. The intrusions that happened in the extension zone at Salton Trough act as the heat sources of the geothermal systems in this area (Younker *et al*., 1982). This extensional system is along the San Andreas Fault and surrounded by granitic and metasediment ridges (Figure 1).

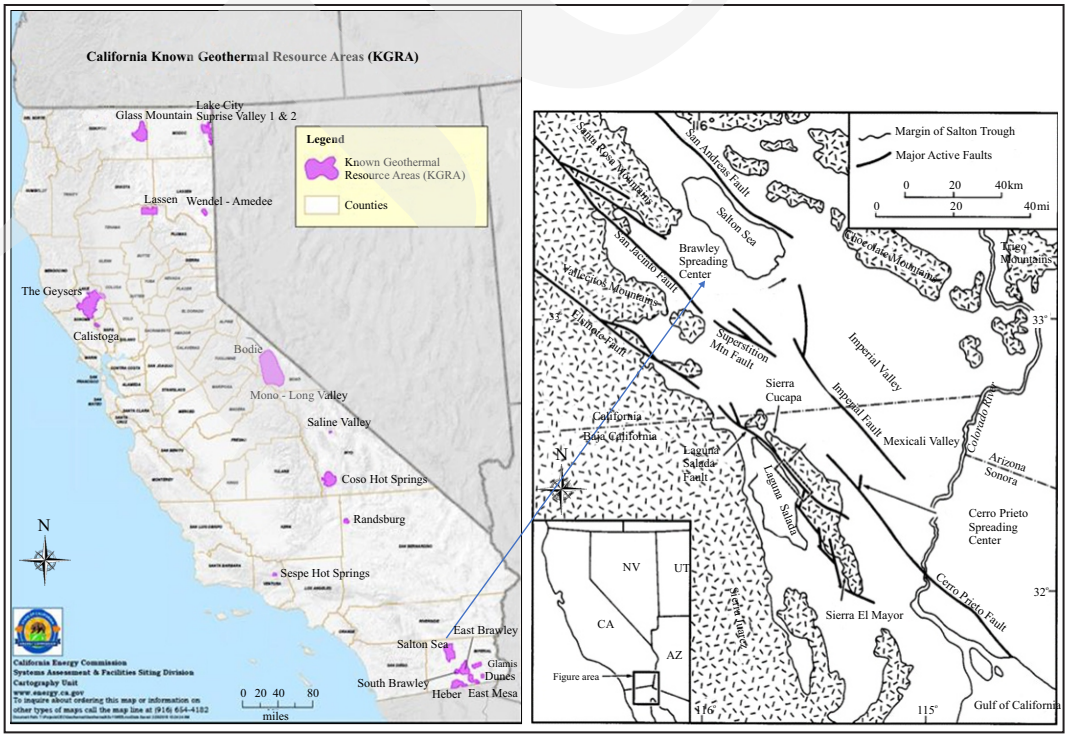

Figure 1. Left, the location of the Salton Sea Geothermal Field (California Energy Commission). Right, simplified geology map of Salton Sea Trough (Mueller and Rockwell, 1995).

Helgeson (1968) described that the trough consisting of Tertiary sediments of lacustrine and deltaic sand shales are overlain by Quaternary alluvium. This accumulation happened in the mid-Pleistocene when the sea level was low representing the long sequence of inland seas since the Pleistocene (de Kamp, 1973).

Younker *et al.* (1982) divided the reservoir rocks into two different types: the upper reservoir comprising sandstones, siltstones, and shales has the indication of minor alterations (silicification and clay mineral reactions), and the lower reservoir extensively altered is proven by the appearance of the epidote and silica filling the reservoir pores replacing calcite and anhydrite. A recent field study at Davis-Schrimpf by Svensen *et al.* (2009) measured that the temperature of the mud pot and gryphons are approximately at 40 - 60^{o}C.

Methods and Materials

Geothermal manifestation on the Salton Sea has been found since early 1540 where multiple indication such as "field of boiling mud", notable thermal springs, and geyser activity were exposed by many earlier researchers (Reath, 2011). The geomorphology condition of the Salton Sea that does not contain much of vegetation makes the remote exploration attempts using satellite and airborne survey possible.

In this study, the surface temperature and emissivity recorded by HyTES were used to identify the anomalous surface temperature and map the mineral as an identifier of surface geothermal manifestations. The thermal infrared sensors were used, because it measured the emitted energy instead of the reflectance. Both processes were executed on the atmospheric corrected HyTES images.

The appearance of ammonia was also tried to be detected from visual inspection, principal component analysis, and band ratio. Detailed explanations of each process are as follows, summarized in Figure 2.

Pre-Processing

In-Scene Atmospheric Compensation (ISAC) was applied to the image for the emissivity and temperature separation. This algorithm corrected the atmospheric path of transmittance and radiance. It also separates the image spectrum by searching for blackbody-like pixels on the image, and calculates radiance and emissivity (Brian, 2002).

Temperature Map

There are numerous papers demonstrating the use of thermal infrared data to investigate the surface temperature anomaly. Coolbaugh *et al.* (2007) used the thermal sensor of ASTER images to detect the anomalies that are associated with hot springs and fumaroles in the Great Basin, Nevada. In this research, the temperature map was used separatedly from HyTES imagery to investigate the anomalous temperature at Davis-Schrimpf Geothermal Field, Salton Sea, California.

Mineral Mapping

As the first step of the mineral mapping, endmembers were extracted from the emissivity

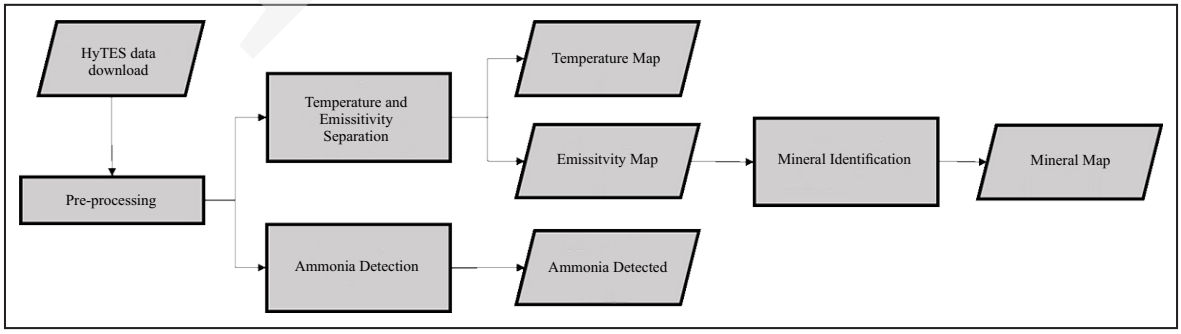

Figure 2. Flow chart of the methodology.

spectrum by performing Minimum Noise Fraction (MNF) transformation (Green *et al.,* 1988). This process was done to remove the noise signal and get the spectrally pure pixels to avoid the mixing endmembers of each mineral. Endmember is a spectral signature of a pixel that represents the surface type from the image, in this case the mineral type.

This transformation is theoretically similar to Principal Component transformation, except that MNF orders the bands by the estimated noise. The bands here are different from the bands of the image captured by the HyTES sensor; these bands represent the principal component/eigenvalue number from the transformation of MNF. The higher the eigenvalue, the higher the signal to noise ratio. Bands are only selected with high eigenvalue with expectation only a small amount of noises included (Figure 3). However, visual checks were also done on every band of the image to inspect if there are any important features that could be found in the higher noised bands.

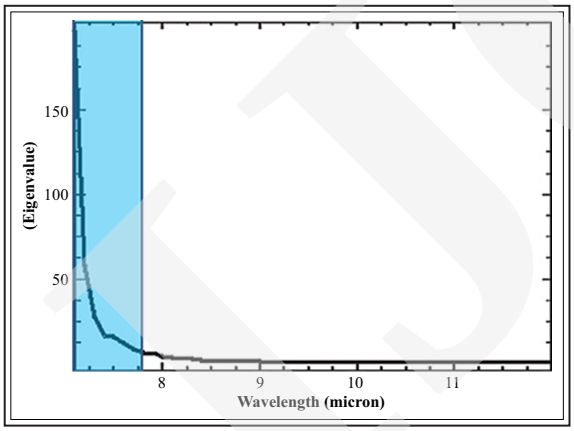

Figure 3. Illustration of band selection (indicated by the wavelength) based on eigenvalue to remove the noise using MNF. Only bands with high eigenvalue are used (highlighted by the blue box).

From the MNF transformation, endmembers were selected from the purest pixels from the Pixel Purity Index (PPI) result and defined manually by referring to the available spectral libraries. In this study, the John Hopkins University Spectral Library was used, ECOSTRESS, as the endmember reference.

After the endmembers were retrieved, Spectral Angle Mapper technique was applied to define the mineralogy of each pure pixel on the image. This method classified the pixel based on the similarity between the spectrum of the endmembers (r) and the target (t). It measures the angle between the vectors of band combination in the feature space (Figure 4) and expressed in Equation 1.

$$SA = \cos^{-1}\left(\frac{\sum_{i=1}^{n} t_i\, r_i}{\sum_{i=1}^{n} t_i^2 \sum_{i=1}^{n} r_i}\right) \quad \text{..... (1)}$$

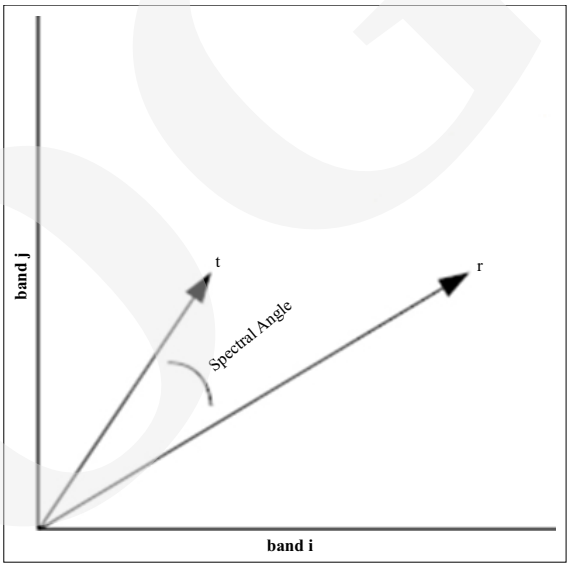

Figure 4. Illustration of spectral angle difference between the endmember spectrum (r) and the target spectrum (t) in two-dimensional feature space.

Ammonia Detection

Multiple approaches were taken on ammonia detection. The first observation carried out the radiance spectra inspection of the ammonia by referring to the spectrum model of ammonia from the MODTRAN model (Ghandehari *et al.,* 2017). As the follow-up, band ratio composite was done by dividing the value at wavelength 10.3 which has the high radiance against 8.3 that has the significant radiance value to get a better recognition from the visual assessment (Figure 5).

The third analysis performed was the band combinations based on Principal Component Analysis and the absorption features of ammonia

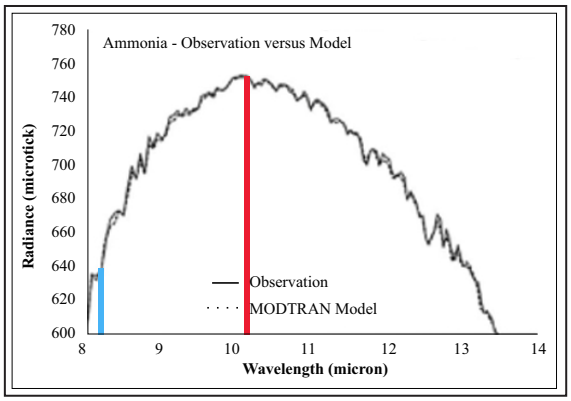

Figure 5. Spectral model of ammonia from radiance spectra (Ghandehari *et al.,* 2017). The blue line indicates the wavelength of low radiance at 8.3, the red line indicates the wavelength of high radiance at 10.3.

at thermal infrared wavelength. Hall *et al*. (2015) detected ammonia using SEBASS and MAGI by highlighting the absorption features within the range of 10 - 11 micrometers (Figure 6). PCA was done on this wavelength range to get both absorption features captured.

Materials

The airborne hyperspectral imagery used in this research is HyTES (2015-02-15_201611_SaltonSea_1_1_02). HyTES imagery has 256 bands between 7.5 and 12 micrometers in the thermal infrared ranges. The sensor was flown on February 15th, 2015, from 2000 m altitude producing an image with 3,41 m pixel size. The image was

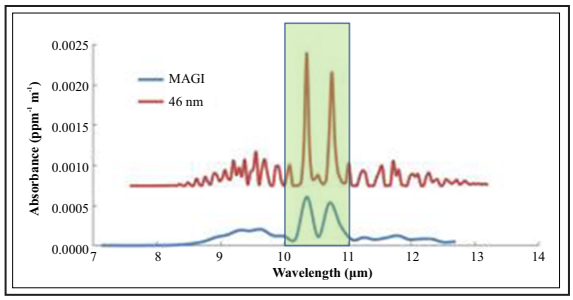

Figure 6. Absorption features of ammonia at 46-nm SEBASS and MAGI (Hall *et al*., 2015).

retrieved from NASA on August 17th, 2018 (Figure 7).

HyTES thermal sensor called Quantum Well Infrared Photodetector (QWIP) produces a high accuracy temperature imagery. According to William (2011), this device is expected to meet the standard of the previously developed JPL thermal infrared spectrometer (QWEST) that has absolute errors on temperature measurements below 0.1°C.

Results

Pre-Processing

The ISAC algorithm separates the temperature image and 256-bands of wavelength emissivity images after removing the atmospheric effect from the original image.

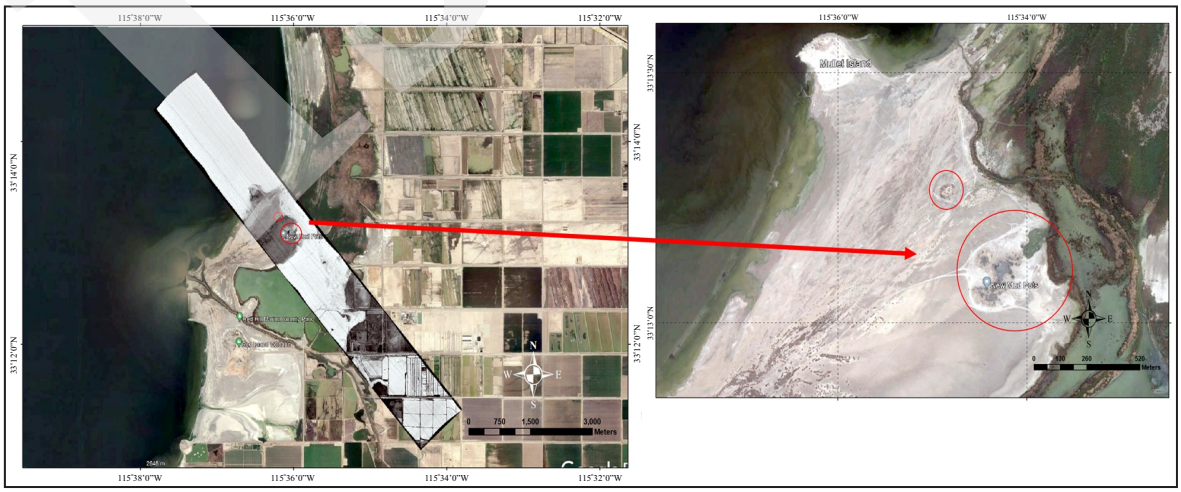

Figure 7. Left, HyTES (2015-02-15_201611_SaltonSea_1_1_02) L1 image. Right, the location of the zone of interest (the mud pots and gryphons) at Davis-Schrimpf Geothermal Field.

Emissivity Map

Based on the statistical result, the quality of the first fifty bands (wavelength range 7.52 - 8.39) of the sensor is not quite good. This was indicated by the quite deviated value at these wavelengths. However, these bands were decided to be kept and used for the next processes, despite the quality being a little bit lower to make sure the features was not missed from the shorter wavelength of the minerals (Figure 8).

Temperature Map

The resulting temperature image from the separation of the HyTES image indicates the ground temperatures of the two targeted zones (more precisely at the mud pots and the gryphons) are high compared to the surrounding area. The estimated temperatures of the mud pots are approximately 314°K (40°C) and higher, which are matched with the temperature from the field measurement (Figure 9).

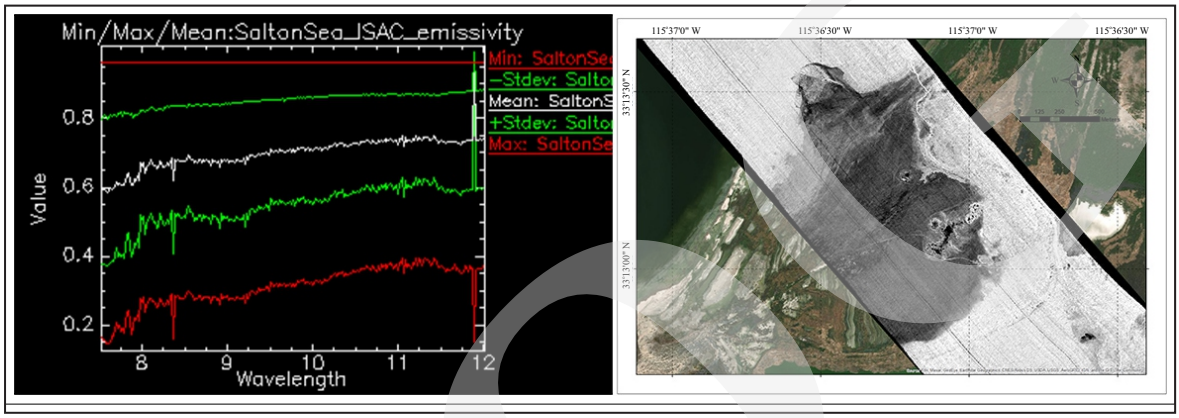

Figure 8. Left, the statistic of emissivity images. Right, the emissivity images represented by one of the bands that has good quality (Band 83).

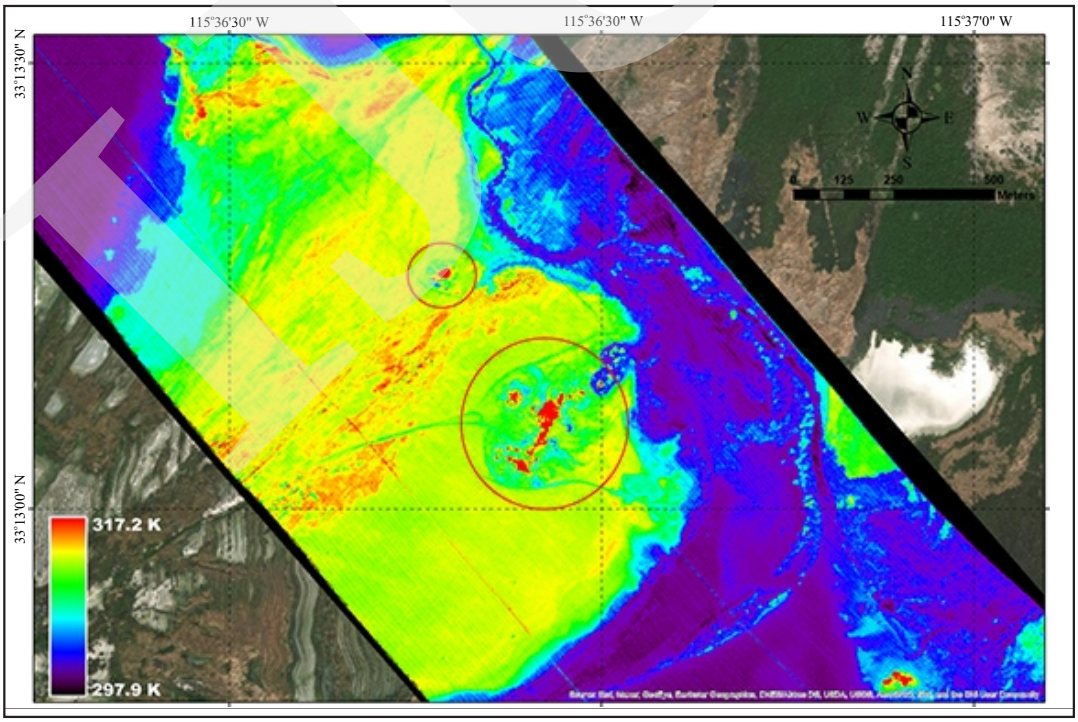

Figure 9. Temperature map of the Davis-Schrimpf Geothermal Field. The high temperatures were found at two circles highlighting the fumaroles.

Mineral Map

MNF

After transforming the emissivity image using MNF, only the first four bands (high signal to noise ratio) were used for further processing. Figure 10 displays the eigen values from the first twenty-five bands and images of the first twelve bands from the total of 256 bands.

According to the eigen value from the statistical results (Figure 10), Bands 1 - 4 show significantly higher values compared to the rest of the bands. This is also supported by the visual inspection of the images from the higher bands that are poorly noised. At some higher bands, the images are still capturing some surface features, but it is decided to take only bands that have eigenvalue higher than 15 to get the least noised result in the further steps of image processing.

End Member Selection

The only pure pixel maintained from the four bands of MNF transformation is shown in Figure 11. From these pixels, four endmembers were retrieved and referenced to the John Hopkins University Spectral Library. From these purest pixels, geothermal indicator minerals such as anhydrite and barites were found in the studied area.

The spectra for barite endmembers from PPI is showing a good match with the library, the first and second absorption features at 8.1 and 8.9 clearly exist. Endmembers of anhydrite and quartz from PPI also show a good reference with the appearance of the absorption features at a similar wavelength as the libraries.

Although the endmember of gypsum was not as good as the other, the spectra are quite comparable by looking at the absorption features around the wavelength of 8.5 (Figure 12).

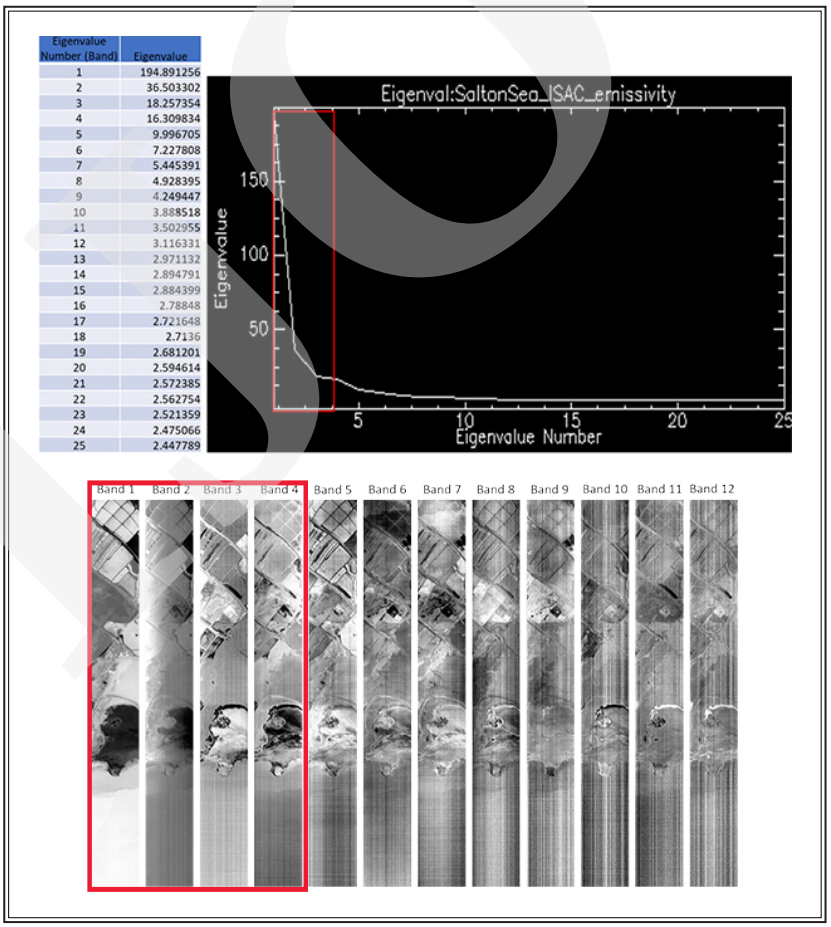

Figure 10. Top left, the recapitulation of the eigen values of the first twenty-five bands. Top right, the plot of eigen values of the first twenty-five bands. Bottom, images of the Bands 1 - 12.

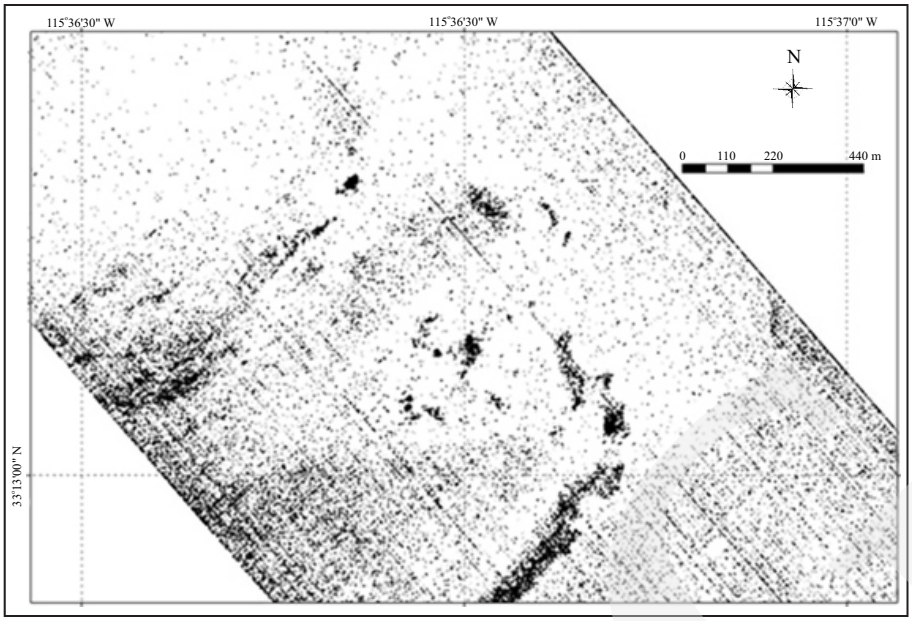

Figure 11. The black coloured pixels indicate the distribution of the pixels that are retained and considered as the purest pixels by the PPI operation.

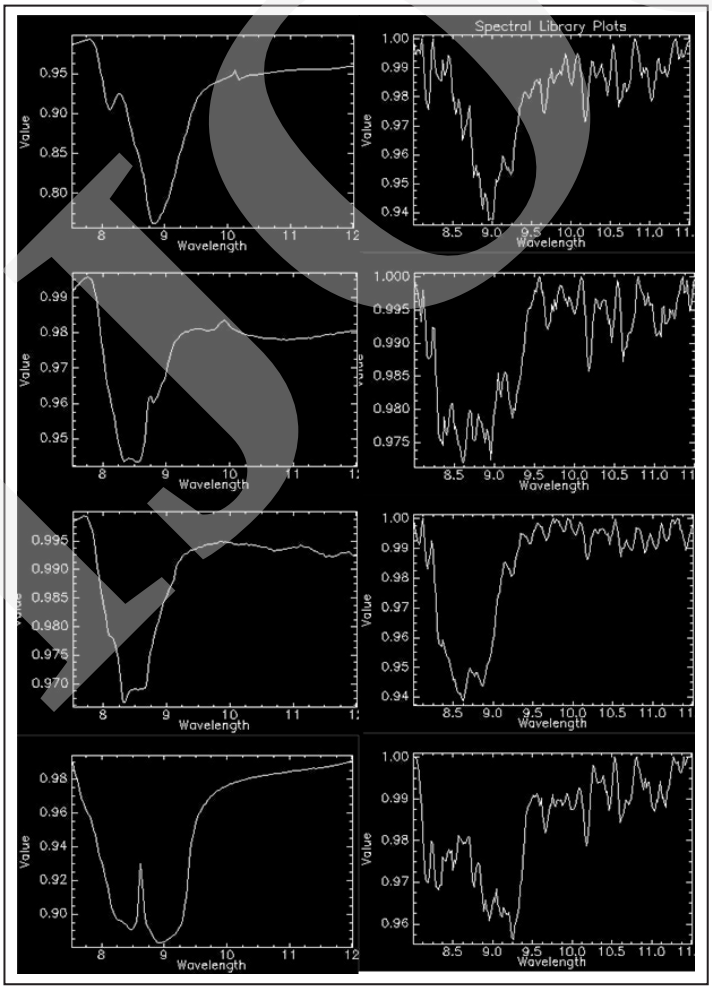

Figure 12. The spectra comparison of each endmember pixels from PPI and JHU Spectral Library.

Spectral Angle Mapper (SAM)

From the collected endmembers, the SAM algorithm classifies the pixels based on the reference, and the results given are shown in Figure 13. In this operation, the maximum angle difference was specified as 0.1 in order to get the result as close as possible to the endmember spectrum. The pixels that had a higher angle than the cut-off were classified as another mineral.

The mineral map displays the distribution of the minerals from endmembers extracted previously. The distribution of anhydrite as the mineral indicator of geothermal in the Salton Sea is scattered in many areas. However, massive accumulations of anhydrite were found surrounding the mud pots and gryphons together with quartz and barites.

Ammonia Detection

The ammonia detection did not provide a result that was expected. Despite several pixels that resemble the radiance spectra of ammonia from previous research were found (Figure 14), the result of band ratio composite and principal component analysis on the pre-defined wavelength range can not display the unique features that represent the appearance of the ammonia in this studied area (Figure 15). There are no unique and significant areas that could represent the ammonia emitted by the mud pots or fumaroles in the studied area.

Discussion

HyTES imagery was able to produce a high-resolution surface temperature and mineral map of the Davis-Schrimpf Geothermal Field. The 3.41m resolution allows us to catch the smaller information inside the geothermal manifestation complex.

Regarding the endmember selections, the lack of quality from the gypsum endmember spectra might be caused by the noises from the MNF band 3 that could be seen visually in Figure 10. However, this band was used to keep the important features in the zone of interest.

From the temperature map, areas with high surface temperature (>40^{o}C) were found precisely at the previously identified mud pot and gryphons. The mineral map was also able to reveal the mineral composition of features and made it possible to describe this from the aerial image.

Overlaying both images gives a better understanding of the suspected areas (Figure 16). The accumulation of Salton Sea geothermal system

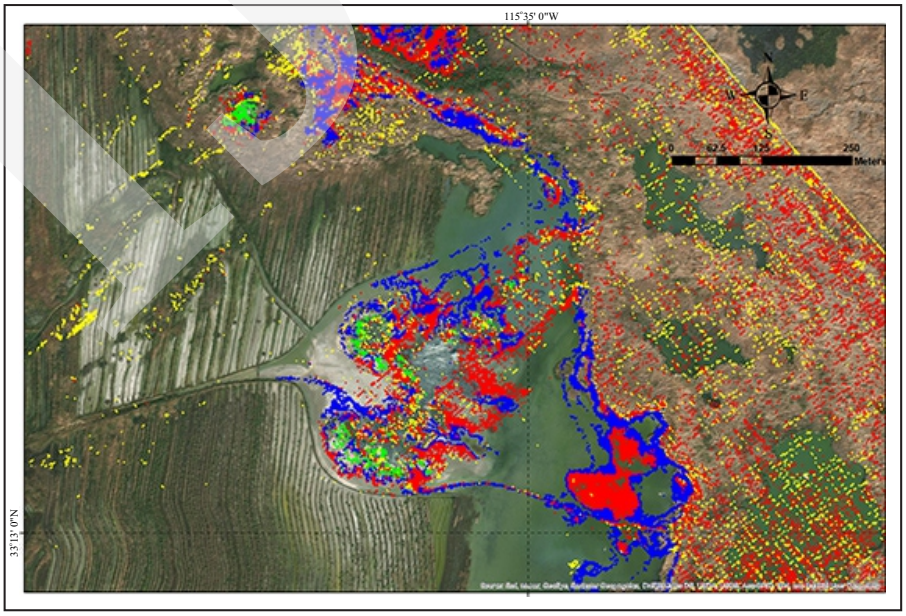

Figure 13. Mineral map from Spectral Angle Mapper.

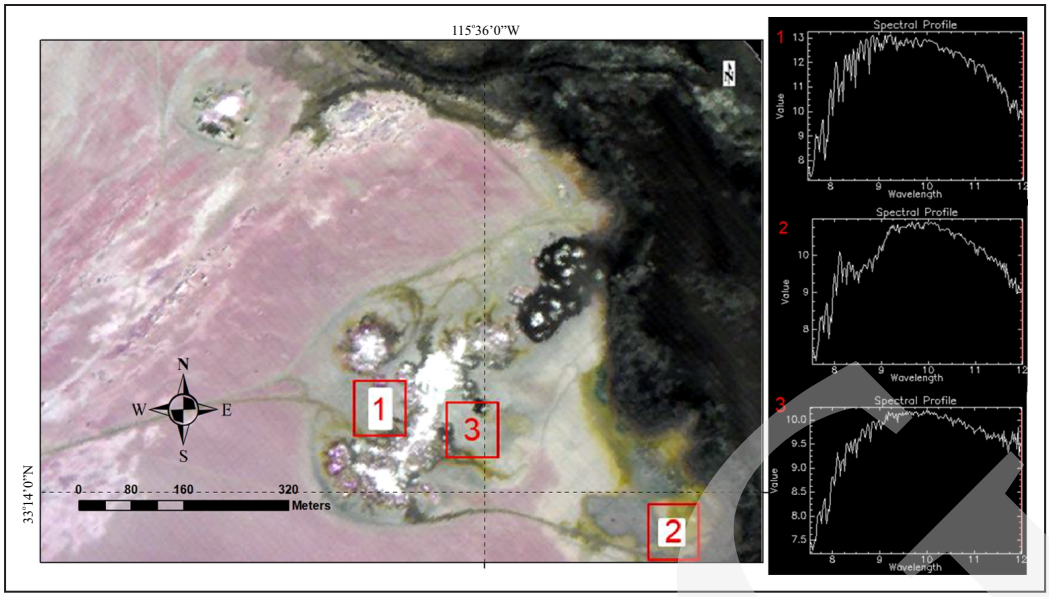

Figure 14. Inspection of the radiance spectra from the surrounding Davis-Schrimpf Field that resembles the spectra of ammonia. The plots on the right side display the radiance spectra of pixels from selected locations.

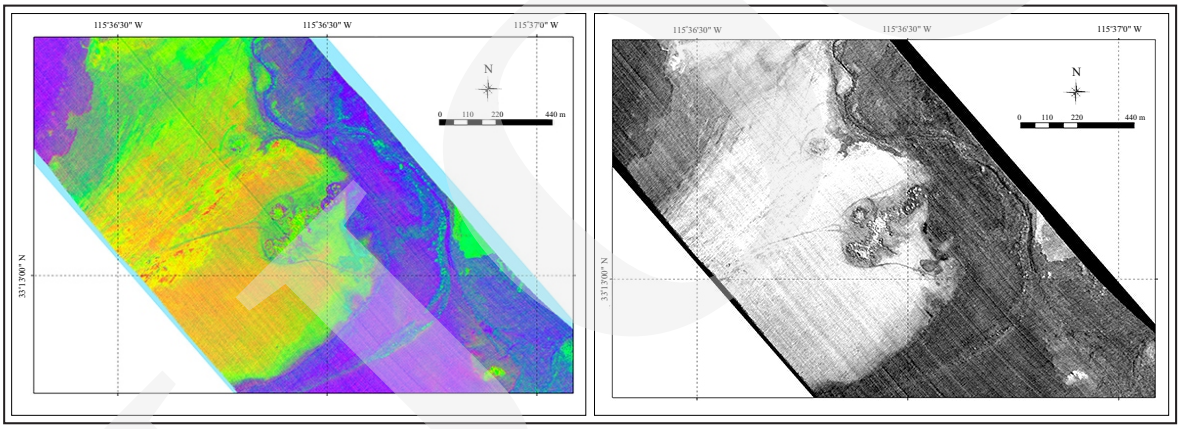

Figure 15. Left, PCA from wavelength 10-11 micrometer of imagery.

mineral indicators, anhydrite and barites were centred in the areas with high temperatures. The fact that barites exclusively occurred in the centre of the features, is consistent with the previous research that stated this mineral occurred at the hydrothermal brine of the Salton Sea Geothermal Field.

Based on the mineralogy, the alteration type of these features is classified as the potassic alteration in the porphyry system. This is shown by the appearance of alteration mineral indicators, quartz and anhydrite, at the centre of the manifestation. From this information, it is confirmed that these features are the direct evidence of surface geothermal addressed in this studied area.

The occurrence of the ammonia was not able to be recognized using simple band manipulations. There is a possibility that the fumaroles and mud pots were not emitting any ammonia during the survey. However, other advanced image processing might also be done instead of only PCA and Band Ratio.

Conclusions

Based on the temperature map, the surface manifestations have similar values with the result of field measurements (>40°C, the mud pots and

gryphons at the Davis-Schrimpf Field were recorded as the hot zones on this map. PPI processes from the first four bands of MNF transformation results were able to generate endmembers that include the geothermal indicator minerals (barite, anhydrite, quartz, gypsum). The mineralogy examination shows that the surface geothermal features are considered as part of the upper reservoir of the Salton Sea geothermal system. This formation is described as slightly altered, proven by the anhydrite that still remained where it was known altered in the lower reservoir formation. To sum up, this research displays the ability of HyTES to identify the surface temperature anomalies and the occurrence of mineral indicators, but failed to diagnose the ammonia emission related to surface geothermal manifestation.

Acknowledgment

The HyTES (The Hyperspectral Thermal Emission Spectrometer) dataset from Jet Propulsion Laboratory California Institute of Technology – NASA, is gratefully acknowledged. Authors would also like to give special gratitude to Dr. Chris A. Hecker from the Faculty of ITC University of Twente for the comments on the initial idea of the article.

References

Bogie, I., Lawless, J., and Morrison, K., 2000. Application of mineral deposit concepts to geothermal exploration. *Proceedings of the World Geothermal Congress*.

Brian, A.G., Robert, C.B., and James, N.S., 2002. New method to optimize atmospheric correction for hyperspectral thermal imaging, *Optical Engineering Journal,* 41 (9), p.2088-2097. DOI: 10.1117/1.1499498.

Coolbaugh, M.F., Kratt, C., Fallacaro, A., Calvin, W.M., and Taranik, J.V., 2007. Detection of geothermal anomalies using Advanced Spaceborne Thermal Emission and Reflection Radiometer (ASTER) thermal infrared images at Bradys Hot Springs, Nevada, USA. *Remote Sensing of Environment,* 106 (3), p.350-359.

De Kamp, P.C. van, 1973. Holocene continental sedimentation in the Salton Basin, California: a reconnaissance. *Geological Society of American Bulletin,* 84, p.827-848.

Der Meer, F. van, Hecker, C., Ruitenbeek, F. van, Der Werff, H. van, De Wijkerslooth, C., and Wechsler, C., 2014. Geologic Remote Sensing for Geothermal Exploration: A Review. *International Journal of Applied Earth Observation and Geoinformation,* 33 (1), p.255-269. DOI: 10.1016/j.jag.2014.05.007.

Ghandehari, M., Aghamohammadi, M., Dobler, G., Karpf, A., Buckland, K., Qian, J., and Koonin, S. 2017. Mapping Refrigerant Gases in the New York City Skyline. *Scientific Reports*, 7. DOI: 10.1038/s41598-017-02390-z.

Green, A.A., Berman, M., Switzer, P., and Craig, M.D., 1988. A Transform for Ordering Multispectral Data in terms of Image Quality with Implications for Noise Removal. *IEEE Transactions on Geoscience and Remote Sensing*, 26 (1), p.65-74.DOI:10.1016/j.rse.2006.09.001.

Hall, J.L., Boucher, R.H., Buckland, K.N., Gutierrez, D.J., Hackwell, J.A., Johnson, B.R., and Young, S.J., 2015. MAGI: A New High-Performance Airborne Thermal-Infrared Imaging Spectrometer for Earth Science Applications. *IEEE Transactions on Geoscience and Remote Sensing*, 53 (10), p.5447-5457. DOI:10.1109/tgrs.2015.2422817.

Harvey, M.C. and Luketina, K., 2014. Thermal Infrared Cameras and Drones: a Match Made in Heaven for Cost- Effective Geothermal Exploration, Monitoring and Development. *New Zealand Geothermal Workshop 2014 Proceedings,* p. 1-4.

Helgeson, H.C., 1968. Geologic and Thermodynamic Characteristics and the Salton Sea Geothermal System, *American Journal of Science*, 266, p.129-166. DOI: 10.2475/ajs.266.3.129.

Johnson, W.R., Hook, S.J., Mouroulis, P., Wilson, D.W., Gunapala, S.D., Realmuto, V.,

Lamborn, A., Paine, C., Mumolo, J.M., and Eng, B.T., 2011. HyTES: Thermal imaging spectrometer development. *IEEE Aerospace Conference*, Big Sky, MT, 2011, p.1-8. DOI: 10.1109/AERO.2011.5747394.

JPL NASA. 2015-02-15_201611_Salton-Sea_1_1_02, The Hyperspectral Thermal Emission Spectrometer – HyTes , L1, August 17, 2018.

Mueller, K. and Rockwell, T., 1995. Late Quaternary activity of the Laguna Salada fault in northern Baja California, Mexico. *Geological Society of America Bulletin,* 107, p.8-18. DOI: 10.1130/0016-7606(1995)107<0008:LQAOTL>2.3.CO;2.

Nishar, A., Richards, S., Breen, D., Robertson, J., and Breen, B., 2016. Thermal infrared imaging of geothermal environments and by an unmanned aerial vehicle (UAV): A case study of the Wairakei - Tauhara geothermal field, Taupo, New Zealand. *Renewable Energy*, 86. p.1256-1264. DOI: 10.1016/j.renene.2015.09.042.

Ramdhan, M.R., 2019. *The investigation of geothermal temperature anomalies and structures using airborne TIR and LiDAR data: a case study in Bajawa area, Indonesia* (M.Sc. Thesis). Enschede, Faculty of Geo-information Science and Earth Observation (ITC), University of Twente. Retrieved from: http://essay.utwente.nl/83454/1/ramdhan.pdf.

Reath, K.A., 2011. *Hyperspectral Thermal Infrared Analysis of the Salton Sea Geothermal Field.* Master Thesis, University of Pittsburgh. Retrieved from: https://d-scholarship.pitt.edu/9188/.

Svensen, H., Hammer, Ø., Mazzini, A., Onderdonk, N., Polteau, S., Planke, S., and Podladchikov, Y., 2009. Dynamics of hydrothermal seeps from the Salton Sea Geothermal System (California, USA) constrained by temperature monitoring and time series analysis, *Journal of Geophysical Research*, B09201. DOI:10.1029/2008JB00624.

van Der Meer, F., Hecker, C., van Ruitenbeek, F., van der Werff, H., de Wijkerslooth, C., and Wechsler, C., 2014. Geologic Remote Sensing for Geothermal Exploration: A Review. *International Journal of Applied Earth Observation and Geoinformation*, 33 (1), p.255-269. DOI: 10.1016/j.jag.2014.05.007.

Younker, L.W., Kasameyer, P.W., and Tewhey, J.D., 1982. Geological, geophysical, and thermal characteristics of the Salton Sea Geothermal Field, California. *Journal of Volcanology and Geothermal Research*, 12 (3-4), p.221-258. DOI:10.1016/0377-0273(82)90028-2.